Available online at www.sciencedirect.com
SCIENCE DIRECT®
Journal of Organometallic Chemistry 689 (2004) 4669–4677
Journal of Organometallic Chemistry
www.elsevier.com/locate/jorganchem

Changes in the hydrogen bonding pattern in ferrocene peptides ☆

Francis E. Appoh, Todd C. Sutherland, Heinz-Bernhard Kraatz *

Department of Chemistry, University of Saskatchewan, 110 Science Place, Saskatoon, Saskatchewan, Canada S7N 5C9

Received 9 March 2004; accepted 8 April 2004
Available online 12 May 2004

Abstract

Disubstituted peptide ferrocenes conjugates were prepared from ferrocenedicarboxylic acid ($Fc(OH)_2$) and glycineethylester. After conversion of the resulting ester $Fc(Gly\text{-}OEt)_2$ **1** into the corresponding acid $Fc(Gly\text{-}OH)_2$ **2** by ester hydrolysis, significant structural changes take place in the way the molecules interact with each other. Complex **1** adopts a 1,3′-conformation showing extensive intermolecular H-bonding forming 1-D chains, whereas complex **2** displays a compact 1,2′-conformation in which the NH on one strand engage in strong intramolecular cross-strand H-bonding involving the amide C=O on the opposite strand. Additional intermolecular H-bonding in **2** allows the formation of a 2-D net. In essence, ester-deprotection allows us to switch the ferrocene conformation and the H-bonding pattern.

Keywords: Ferrocene; Amino acid; Electrochemistry; H-bonding; pK_a

1. Introduction

Peptides are valuable building blocks for the formation of larger assemblies. Its architecture can be controlled by choice of the amino acid sequence which in turn will control the inter- or intramolecular hydrogen bonding and electrostatic interactions [1–3]. Intermolecular H-bonding has allowed the formation of ordered peptidic systems, such as peptide tubes [4], and has been exploited in the crystal engineering of non-biological materials [5]. The incorporation of redox active organometallic moieties into such non-covalent peptidic supramolecular frameworks would be highly useful, allowing the rational design of novel biomolecular sensing and switching devices [6,7]. Ferrocene–peptide conjugates are particularly useful in this regards. The ferrocene group is readily incorporated into a peptidic framework under very mild conditions [8]. Its redox potential is influenced by the peptide's secondary structure, and by structural changes due to substrate binding to the peptide [8].

In amino acid and peptide ferrocene conjugates, the proximity of the two Cp rings allows for very facile intramolecular H-bonding involving the amide groups of two amino acid esters on the two opposite Cp rings, thereby imposing structural rigidity. Recent crystallographic studies by Hirao and co-workers [9] and Metzler-Nolte and co-workers [10] of 1,1′-disubstituted ferrocene derivatives in which both Cp rings have a podand amino acid ester or peptide ester substituent exhibit strong intramolecular H-bonding, as was proposed by Herrick et al. [11] earlier based on solution studies. In some cases, the systems assemble further into chiral supramolecular assemblies [9]. However, the cross-strand intramolecular H-bonding is not affected by the interactions with neighboring molecules. And even the presence of strongly H-bonding acids does not disrupt the intramolecular H-bonding [9e]. Monosubstituted ferrocene–peptides conjugates assemble to 1-D or 2-D structures via intermolecular H-bonding, while disubstituted ferrocene–peptide conjugates engage in strong intramolecular H-bonding, which then may assemble into larger structures [6–10]. Although, Erker's 1,1′-bis-valinemethylester [12], adopts a 1,2′-conforma-

☆ Supplementary data associated with this article can be found, in the online version, at doi: 10.1016/j.jorganchem.2004.04.017.

* Corresponding author. Tel.: +1-306-966-4660; fax: +1-306-966-4730.
E-mail address: kraatz@skyway.usask.ca (H.-B. Kraatz).

0022-328X/$ - see front matter © 2004 Elsevier B.V. All rights reserved.
doi:10.1016/j.jorganchem.2004.04.017

tion similar to that displayed by Hirao's and Metzler-Nolte's systems, the system exhibits no intramolecular H-bonding. We were surprised by this finding.

As part of our ongoing program into redox-active bioconjugates [6b,8], we proceeded to investigate the role of the substituent on the electrochemical and structural properties of the system and now present our results. We chose to focus on 1,1′-bis(glycine)ferrocenes having two podand glycine substitutents. This system was used before in transmetallations reactions but was never structurally characterized [13]. Although disubstituted ferrocenes in general are conformationally highly adaptable, 1,2′- and 1,3′-conformers are sterically preferred, whereas in the presence of strong intermolecular interactions the eclipsed 1,1′-conformer can be favored [14]. For example, ferrocene dicarboxylic acid ($Fc(OH)_2$) crystallizes as a strongly H-bonded dimer [15]. However, its H-bonding is easily disrupted giving the sterically preferred 1,2′- and 1,3′-conformers [16].

The challenge is clear: *Can the H-bonding pattern in 1 1′-bis-amino acid-substituted ferrocenes be influenced? And if so, this raised the questions as to what are the governing principles determining the H-bonding pattern?* Previous reports show that the 1,2′-conformation is preferred for bis-substituted Ferrocenoyl (Fc)-peptide and amino acid esters resulting in intramolecular H-bonding (vide supra) [9–11]. The structure of the amide $Fc(Gly\text{-}NH_2)_2$ was recently reported by Mingos, showing the now familiar cross-strand intramolecular H-bonding involving the amide NH and C=O and engaging in additional intermolecular interactions through the terminal NH_2 amide, resulting in a complex H-bonding network [17].

Here, we focus on two glycine–ferrocene conjugates, one of which is ester protected $Fc(Gly\text{-}OEt)_2$, (**1**), the other is unprotected $Fc(Gly\text{-}OH)_2$, (**2**). We observe significant structural changes between the ester and the free acid. Deprotection of the ester to the free acid goes hand in hand with a drastic change in the H-bonding pattern from an intermolecular H-bonding to an intramolecular H-bonding pattern in the solid state. We are presenting the results of a combined NMR and crystallographic study, providing details of the solution and solid state behavior of these compounds. The results have significance in the context of crystal engineering [18]. Switching the H-bonding pattern of ferrocene–glycine conjugates is a significant result that may potentially allow their use as robust H-bonding and redox-active supramolecular building blocks [19].

2. Experimental

2.1. General procedure

All syntheses were carried out in air unless otherwise indicated. CH_2Cl_2 and $CHCl_3$ (BDH; ACS grade) used for synthesis, FT-IR and electrochemistry were dried (CaH_2), and distilled under N_2 prior to use. Acetone, EtOAc, CH_3CN, MeOH, diethyl ether (BDH; ACS grade), hexanes (Fischer; HPLC grade), $CHCl_3$ and CH_2Cl_2 used for the purpose of purification were used as received. $CDCl_3$ and CD_3CN (Aldrich) were dried by, and stored over molecular sieves (8–12 mesh; 4 Å effective pore size; Fisher) before use. Acetone d-6 (MSD) was used as received. EDC, HOBt, H-Gly-OEt · HCl (Aldrich), $MgSO_4$, $NaHCO_3$ (VWR), and $Fc(OH)_2$ (Strem) were used as received. Et_3N (BDH; ACS grade) used in Fc-amino acid couplings was dried by molecular sieves when used in stoichiometric quantities. For column chromatography, a column with a width of 2.7 cm (ID) and a length of 45 cm was packed 18–22 cm high with 230–400 mesh silica gel (VWR). For TLC, aluminum plates coated with silica gel 60 F_{254} (EM Science) were used. NMR spectra were recorded on either a Bruker AMX-300 spectrometer operating at 300.135 MHz (^1H) and 75.478 MHz ($^{13}C\{^1H\}$), or on a Bruker AMX-500 spectrometer operating at 500 MHz (^1H) and 125 MHz ($^{13}C\{^1H\}$). Peak positions in both ^1H and ^{13}C spectra are reported in ppm relative to TMS. ^1H NMR spectra of Fc-peptides are referenced to the CH_2Cl_2 resonance (δ 5.32 ppm) of an external standard ($CDCl_3$/CH_2Cl_2). ^1H spectra of all other compounds are referenced to the residual $CHCl_3$ signal. All $^{13}C\{^1H\}$ spectra are referenced to the $CDCl_3$ signal at δ 77.23 ppm.

2.2. Preparation of $Fc(Gly\text{-}OEt)_2$ (*1*)

To a stirring mixture of $Fc(COOH)_2$ (0.85 g, 3.0 mmol) and HOBt (1.01 g, 6.6 mmol) in CH_2Cl_2 (25 ml) at room temperature, solid EDC (1.27 g, 6.6 mmol) is added, causing the orange slurry to slowly change into a clear solution. In a separate flask, H-Gly-OEt · HCl (1.09 g, 6.6 mmol) is dissolved in CH_2Cl_2 (10 ml) and Et_3N (0.5 ml, 6.6 mmol) and is then added to the stirring reaction mixture. After stirring overnight, the reaction solution is washed consecutively with aqueous solutions of saturated $NaHCO_3$, 10% citric acid, saturated $NaHCO_3$ and finally with distilled water. The organic phase is dried by anhydrous Na_2SO_4, filtered, and the solvent removed under reduced pressure giving the crude orange product. The product is purified by column chromatography ($R_f = 0.3$; hexane/EtOAc/$CHCl_3$ 1:1:2) giving an orange solid. Yield: 61%. (0.80 g). Elemental analysis, Calc. for $C_{20}H_{24}N_2O_6Fe$ C, 54.07; H, 5.45; N, 6.31; C, 52.6; H, 5.2; N, 6.1. LR-MS (FAB+, NBA): Calc. 444; Found 445 $[M + 1]^+$. HR-MS (FAB+, NBA): Calc. for $C_{20}H_{25}N_2O_6Fe$ $[M + 1]^+$: 445.1062, Found: 445.1062. FT-IR (cm^{-1}, 6 mM $CHCl_3$): 3440 (s, br), 1743 (s, C=O ester), 1632 (s, Amide I). UV–Vis ($CHCl_3$, λ_{max} in nm, ε in $cm^{-1}M^{-1}$): 443 (270). ^1H NMR (DMSO-d_6, δ in ppm): 7.97 (1H, t, $J = 5.9$ Hz, NH,), 4.74 (2H, s, H^o Cp), 4.45 (2H, s, H^m Cp), 4.10 (2H, q,

$J = 7.1$ Hz, OCH_2 ester), 3.88 (2H, d, $J = 5.9$ Hz, CH^{α}-Gly), 1.19 (3H, t, $J = 7.1$ Hz, CH_3 of ester). $^{13}C\{^1H\}$ NMR (δ in ppm, DMSO-d_6): 171.1, 170.1 (C=O), 77.5 (C^i), 73.0 (C^o), 70.5 (C^m), 61.4 (CH_2–O ester), 41.8 (C^{α} of Gly), 15.0 (CH_3 ester).

2.3. Preparation of Fc(Gly-OH)$_2$ (2)

Compound **1** (550 mg, 1.2 mM) was dissolved in 40 ml dioxane:water (1:1) and NaOH (100 mg, 2.4 mM) was added in ice. The reaction mixture was stirred at room temperature for 10 min and allowed to stand undisturbed for 1 h. The disappearance of the starting material was followed by TLC using methanol/$CHCl_3$ (5:95). The solution was acidified with 1N HCl to pH 2–3. The aqueous reaction mixture was then extracted with EtOAc (3×50 ml). The organic layer was dried over anhydrous Na_2CO_3, filtered, and the solvent removed under reduced pressure giving the crude orange product. The product is purified by column chromatography ($R_f = 0.25$ AcOH/MeOH/CH_2Cl_2 1:2:17) giving 490 mg of an orange solid. Yield: 95%. Elemental analysis, Calc. for $C_{16}H_{16}N_2O_6Fe \cdot 1/2\ CH_2Cl_2$ C, 46.02; H, 3.98; N, 6.51; C, 45.9; H, 3.6; N, 6.6. HR-MS (FAB) found [M + H$^+$] 389.0417, calculated for 388.158. FT-IR (cm^{-1}, KBr): 3385 (s, br), 1715 (s, C=O ester), 1593 (s, Amide I). UV–Vis (CH_3OH, λ_{max} in nm, ε in cm^{-1} M^{-1}): 444 (245). ^1H NMR (DMSO-d_6, δ in ppm): 12.69 (1H, br s, OH), 8.21 (1H, br s, NH), 4.80 (2H, s, H^o Cp), 4.43 (2H, s, H^m Cp), 3.85 (2H, br s, H$^{\alpha}$-Gly). ^{13}C NMR (DMSO-d_6, δ in ppm) 172.7, 169.9 (C=O), 77.6 (C^i), 72.8 (C^o), 70.5 (C^m), 41.8 (C^{α}).

2.4. Electrochemical studies

All electrochemical experiments were carried out at room temperature (22 ± 1 °C) on a CV-50W Voltammetric Analyzer (BAS) in aqueous solution using a conversional three electrode cell system of glassy carbon (BAS 3.0 mm diameter) as working electrode, Pt wire as counter electrode and Ag/AgCl (3.0M NaCl, BAS) as reference electrode. Electrochemical measurements were made on 0.5 mM of the compounds in MeOH containing 0.1 M TBAP as supporting electrolyte. For the cyclic voltammetric (CV) studies the scan rates was 100 mV/s whiles for the differential pulse voltammtry experiments a scan rate of 20 mV/s and pulse amplitude of 50 mV was used. A stream of argon was passed over the solution prior to taking the scans. IR compensation was applied to all voltammetric measurements. The carbon electrodes were cleaned by polishing on microcloth pads with aluminum slurry and rinsed with copious amount of Millipore water. To ensure reproducibility, the working electrode was also cleaned in between runs.

2.5. pK_a determination by cyclic voltammetry

For the determination of the acid–base property of compound **2** studies was studied by cyclic voltammetry on a 0.5 mM solution of the compound in 5%MeOH-aq. phosphate buffers of pH 2–8.0, prepared with H_3PO_4, Na_2HPO_4, KH_2PO_4 to an ionic strength of 0.2 M. Where necessary the pHs were adjusted by the addition of 1N HCl or 1N NaOH. pH measurements were carried out using a Accu-pHast combination glass electrode and standardized with VWR pH 4 and 7 buffer standards. CVs were scanned in the potential range of 0.4–1.1 V versus Ag/AgCl at a scan rate of 100 mV s^{-1}.

2.6. X-ray crystallography

Suitable crystals of Fc(Gly-OH)$_2$ were obtained by a slow diffusion of hexane into a methanolic solution of **1** at room temperature. Yellow needles suitable for X-ray crystallography were deposited after a few days. Crystals of Fc(Gly-OEt)$_2$ were obtained from a hexane layered solution of compound **2** in CH_2Cl_2. Both compounds were mounted onto glass fibres. Data for compounds **1** and **2** were measured using a Bruker P4 SMART equipped with a rotating anode and a 1000 CCD using Mo Kα radiation (graphite monochromated) with ω scans. Both structures were solved using direct methods [20]. For **1** and **2**, all non-hydrogen atoms were refined anisotropically using full-matrix least-squares on F^2. The real hydrogen atom positions were located within the difference map. Then all hydrogen atoms were placed on calculated positions and included in the refinement. For compound **1**, the final R-value was 0.0242 for 1414 reflection with $I > 2\sigma(I)$ (4323 total reflections). The final R value for compound **2** was $R = 0.0567$ for 2857 reflection with $I > 2\sigma(I)$ (28 286 total reflections). All crystallographic details have been summarized in Table 1. The crystal data has been deposited at the Cambridge Crystallographic Data base as CCDC 233298 (for **1**) and CCDC 2332999 (for **2**).

3. Results and discussion

3.1. Synthesis and characterization of Fc-dipeptides

Coupling of H-Gly-OEt to ferrocene dicarboxylic acid (Fc(OH)$_2$ using the EDC/HOBt procedure adapted for Fc-conjugates [21] (Scheme 1) resulted in the formation of the desired 1,1′-ferrocenoylglycineethylester (**1**) as an orange solid which crystallizes readily from CH_2Cl_2. This procedure differs from Wenzel's procedure for the formation of **1**, in which the common acid chloride methods was used.

Base de-protection of the ester gives the free 1,1-ferrocenoylglycine acid (**2**) in nearly quantitative yields.

Table 1
Summary of crystallographic data for compounds **1** and **2**

	1	**2**
Chemical formula	$C_{20}H_{24}FeN_2O_6$	$C_{16}H_{16}FeN_2O_6$
Formula weight	440.23	388.16
Crystal size (mm)	$0.68 \times 0.07 \times 0.04$	$0.37 \times 0.20 \times 0.13$
Crystal system	Orthorhombic	Orthorhombic
Space group	*Pbca*	*Fdd*2
a (Å)	18.6408(11)	12.9218(15)
b (Å)	9.8489(6)	23.993(3)
c (Å)	21.7130(13)	9.9580(12)
α (°)	90	90
β (°)	90	90
γ (°)	90	90
V (Å)^3	3986.3(4)	3087.3(6)
Z	8	8
$D_{calc.}$ (g/cm^3)	1.467	1.670
T (K)	193(2)	193(2)
λ (nm)	0.71073	0.71073
μ (mm$_{-1}$)	0.796	1.015
$R(I > 2\sigma(I))a$	0.0567	0.0228
wR (all data)*b*	0.1489	0.0557
Data/restraints/parameter	4068/0/262	1475/1/115
Goodness-of-fit on F^2c	1.101	1.088

$R = \sum ||F_o| - |F_c|| / \sum |F_o|$; $R_w = \left[\sum w(F_o^2 - F_c^2)^2 / \sum w(F_o^4)\right]^{1/2}$; $w = [\sigma^2(F_o^2) + (0.0879P^2 + 0.0229P]^{-1}$ where $P = \left[\mathrm{Max}(F_o^2, 0) + 2F_c^2\right]/3)$.

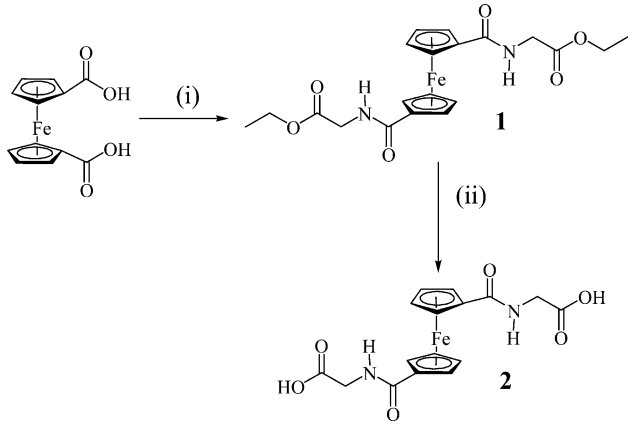

Scheme 1. Synthesis of 1,1′-ferrocenoylglycineethylester (**1**) and 1,1′-ferrocenoylglycine (**2**): (i) (a) HOBt, EDC in CH_2Cl_2 and (b) H-Gly-OEt · HCl, NEt_3 in CH_2Cl_2; (ii) NaOH in dioxane/water (1:1).

The reaction can be conveniently followed by TLC. Compounds **1** and **2** were characterized by ^{1}H- and ^{13}C{^{1}H} NMR spectroscopy, mass spectrometry (MS) and elemental analysis. ^{1}H NMR assignments were made on the basis of chemical shift, relative integration, signal multiplicity and comparison with similar compounds. Loss of the ethyl group is also indicated in the ^{1}H NMR spectrum which shows a lack of the signals of the Et group (δ 4.10 and 1.19 in DMSO-d$_6$) for compound **2**. In addition, upon de-protection of **1**, a broad resonance at δ 12.69 appears and is assigned to the acid OH group in **2**. Furthermore, the chemical shift of the amide NH group changes from δ 7.97 in **1** to δ 8.21 in **2**.

The IR spectrum of the ester **1** in solution shows a typical ester band at 1743 cm^{-1}. Upon de-protection, the newly formed acid group is readily detected by its characteristic IR band at 1715 cm^{-1}. In the ^{13}C NMR spectrum, the new acid carbonyl appears at δ 171.1 compared to δ 172.7 for the ester. Electronic effects due to the different substituents (–OH versus –OEt), if any, are insignificant, as shown by a lack of effects exerted on the chemical shift of the *ipso*-C in the ^{13}C NMR and similar λ_{max} for the Fc-based transition at 450 nm.

The amide NH resonances of both complexes **1** and **2** experience a temperature dependent chemical shift, as would be expected for compounds able to engage in H-bonding (see Supplemental). In DMSO-d6, the amide NH resonances of **1** and **2** exhibit temperature dependences of 6.3 and 8.1 ppb K^{-1}, respectively, for a 1 mM solution in the temperature range between 273 and 310 K. Both compounds clearly exhibit a temperature dependence that is characteristic of H-bonding. For intermolecular H-bonding, an increase in concentration should increase the temperature dependence. However, in both complexes, the temperature dependence appears concentration independent. Similar temperature dependences have be observed in other H-bonded Fc-peptide systems [8,10,22]. The temperature dependence of the NH shift for complex **1** in $CDCl_3$ is slightly lower (4.2 ppb K^{-1}). However, under these conditions, the system exhibits a slight concentration dependence (50 mM; 6.2 ppb K^{-1}), indicating possible additional intermolecular H-bonding for **1** in solution. Related experiments using the free acid **2** were not possible due to its insolubility in $CDCl_3$.

3.2. Solid state structure

Single crystals of compounds **1** and **2** were obtained by diffusion methods giving yellow needles of 1 and yellow–orange crystals of **2** suitable for X-ray crystallography. The crystal structure of the glycine ester **1** is shown in Fig. 1. The Fc substitution pattern shows the two podand glycineethylesters in a 1,3′-conformation. The absence of the 1,2′-conformation with its cross-strand H-bonding motif in this system is surprising and was not be predicted based on the available literature [6,7,9–13]. Other features displayed by compound **1**, such as the co-planarity of the Cp rings (1.8°) and the small Cp-amide twist angle (Cp1-amide: 14.1° and Cp2-amide 15.2°) are common to many ferrocene amides [8,9c,23,24]. The Cp–C(O) distances of 1.482(5) and 1.487(5) Å for C(1)–C(11) and C(6)–C(16), respectively, are within the range of other Fc-amino acids and peptides and simple Fc-amides [18–24]. Similarly, the amide C=O (O(1)–C(1) = 1.235(5) Å, O(4)–C(6) = 1.230(4) Å) and amide C–N (C(1)–N(1) = 1.326(5) Å, C(6)–N(2) = 1.344(5) Å) bond distances are normal compared to related Fc-amino acids and

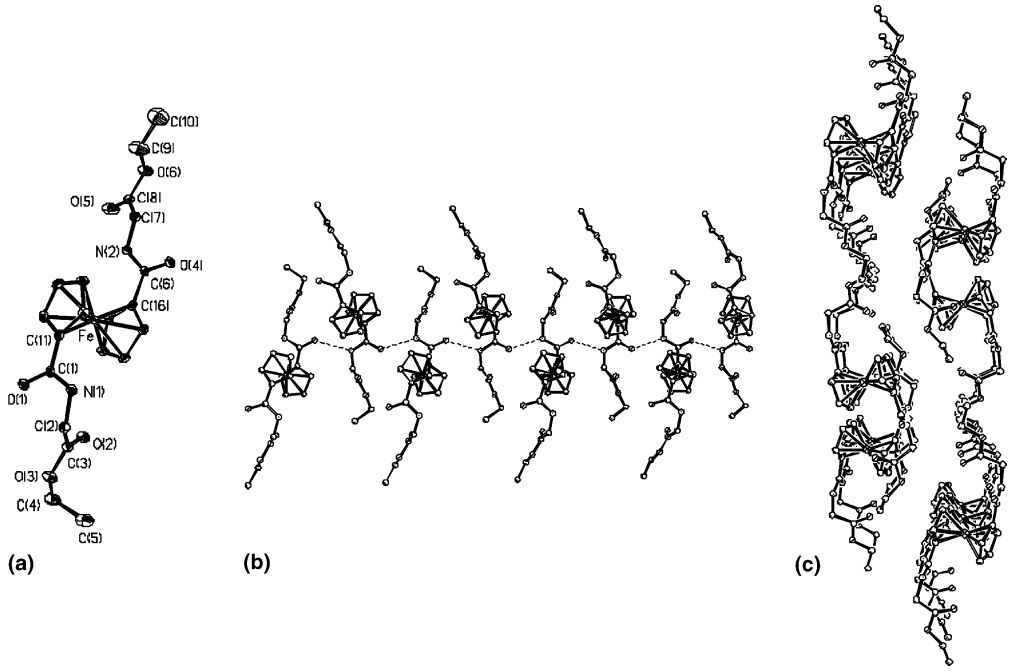

Fig. 1. (a) ORTEP drawing of compound **1** showing the 1,3′-substitution of the ferrocene group. Ellipsoids are drawn at the 30% probability level. All hydrogen atoms are omitted for clarity; (b) formation of a one-dimensional H-bonded polymeric chain involving H-bonding of N(1) and O(1) of adjacent molecules; (c) packing of the one-dimensional chains to give a layered structure. The separation between layers is 4 Å and the thickness of a double-layer is 11.4 Å. Selected distances and angles: Fc–C_{mean} = 2.0442(4) Å, Cp–C(1) = 1.482(5) Å, C(6)–O(4) = 1.230(4) Å, Cp–C(6) = 1.487(5) Å, C(1)–N(1) = 1.326(5) Å, C(6)–N(2) = 1.344(5) Å, C(1)–O(1) = 1.235(5) Å, O(1)···N(1A) = 2.839(5) Å; (b) angles: Φ_1 C(1)–N(1)–C(2)–C(3) = 65.4(4)°, Cp–Fe–Cp = 1.8(5)°; Ψ_1 N(1)–C(2)–C(3)–O(3) = −158.4(3)°, amide twist Cp1-amide = 14.1°, Φ_1^* C(6)–N(2)–C(7)–C(8) = −69.9(5)°, amide twist Cp2-amide 15.2°, Ψ^* N(2)–C(7)–C(8)–O(6) = 162.3(3)°.

peptides. The molecule interacts with its adjacent neighbors through H-bonding, resulting in the formation of a 1-dimensional chain H-bonded chain, in which O(1) interacts with the N(1) of the Gly group of an adjacent molecule (O(1)···N(1) = 2.839(5) Å, Fig. 1(b)). Interestingly, the amide group on the other Cp ring is not involved in H-bonding and is well separated from other molecules (ca. 4 Å). This H-bonding pattern is reminiscent of that reported by Hirao and coworkers for the monosubstituted Fc-Ala-Pro-OEt with alternating up–down orientation of the molecules [6a]. The resulting dihedral angles of the podand glycine ethylester which is involved in H-bonding are $\Phi 1 = 65.4(4)°$, $\Psi 1 = -158.4(3)°$.

In comparison, those of the other substituent not involved in H-bonding are $\Phi 1^* = -69.9(5)°$, $\Psi 1^* = 162.3(3)°$. The individual chains are separated from each other by 4 Å and form a layered structure with a layer thickness of 11.4 Å, as shown in Fig. 1(c).

The crystal structure together with selected bond angles and distances of the free acid **2** are shown in Fig. 2. In contrast to the ethyl ester **1**, compound **2** is centrosymmetric with strong intramolecular H-bonding between the two podand substitutents forcing the ferrocene framework into the now familiar 1,2′-orientation (N···O(2A) and O(2)···N(A) = 2.875(3) Å, observed for other disubstituted ferrocene–peptide conjugates

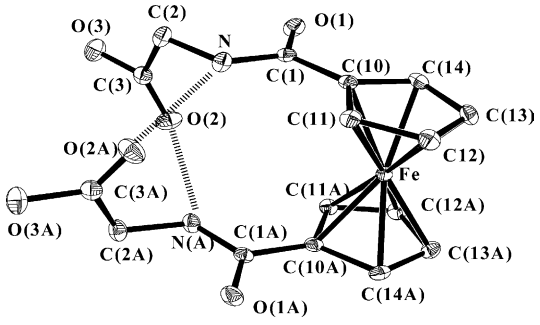

Fig. 2. ORTEP drawing of compound **2** showing the 1,2′-substitution of the ferrocene group. The intramolecular hydrogen bonding distances between N and O(2A) and N(A) and O(2) is 2.875(3) Å. Ellipsoids are drawn at the 30% probability level. All hydrogen atoms are omitted for clarity. Selected bond distances and angles: Fc–C_{mean} = 2.044(2) Å, Cp–C(1) = 1.472(3) Å, C(1)–N = 1.327(3) Å, C(1)–O(1) = 1.246(2) Å, O(2)–C(3) = 1.205(3) Å, O(3)–C(3) = 1.314(3) Å, O(2)···N(A) = 2.875(3) Å, Φ_1 C(1)–N–C(2)–C(3) = 79.0(2)°, Cp–Fe–Cp = 0.9°, Ψ_1 N–C(2)–C(3)–O(3) = −178.60(18)°, amide twist Cp1-amide = 2.9°.

[6,7,9,10,12,17]. This provides a rigid framework, in which the amide twist is reduced considerably (2.9°).

The resulting dihedral angles Φ_1 and Ψ_1 are significantly different from the ethyl ester ($\Phi_1 = 79.0(2)°$ and $\Psi_1 = -178.60(18)°$). The Fc–C=O group establishes intermolecular H-bonding contacts with the acid O–H

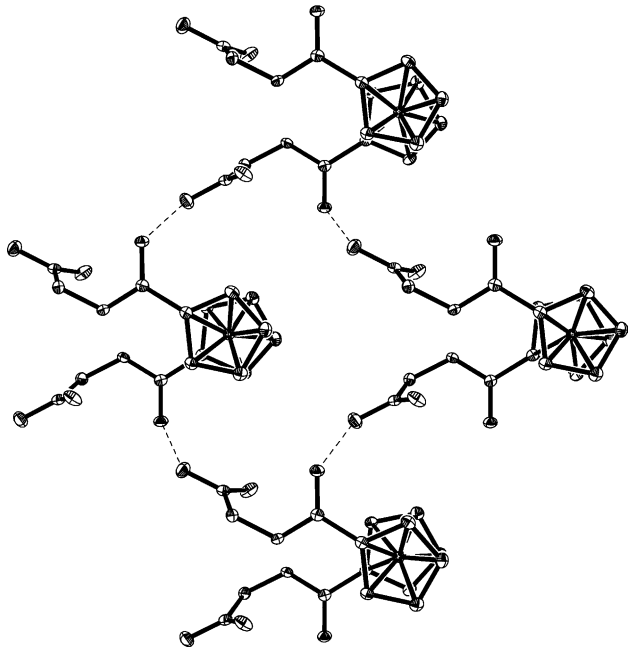

Fig. 3. H-bonding interactions between adjacent molecules involving the interaction of the Fc–C═O group with the acid OH ($O(1)\cdots O(3^*) = 2.620(3)$ Å).

of adjacent neighbors with a H-bonding distance of $O(1)\cdots O(3^*) = 2.623(3)$ Å (Fig. 3). Similarly the amide NH_2 in Mingos' amide derivative engages in intermolecule interactions with adjacent molecules [17]. The intramolecular H-bonding interaction involving the two amide NH and the two acid C═O on opposite Cp rings is responsible for the conformation of the acid OH and the Fc–C═O and forces them into a conformation which allows the formation of a two-dimensional H-bonded network, in which there are strong interactions between the Fc–C═O and the OH groups of adjacent molecules ($d(O(1)\cdots O(3^*) = 2.620(3)$ Å). In addition, there are weak O···H–C interactions between O(1) and H(12) on the Cp ring, which may support the structural motif provided by the stronger C═O···H–O H-bond. Weak C–H···O and C–H···N H-bonding interactions are well documented to be important factors in stabilizing and sometimes even controlling the structure in the solid state [25].

3.3. Electrochemical characterization

Fig. 4 shows the cyclic voltammograms (CVs) and the differential pulse voltammograms (DPVs) of compounds **1** and **2** in methanol. The CV shows that both compounds exhibit a fully reversible one electron oxidation with a half-wave potential $E_{1/2}$ for both compounds at 805(3) mV with anodic to cathodic peak separation (ΔE about 80–90 mV) and the ratio of peak currents of close to unity. The oxidation peak potential E_p for both compounds is E_p of 796(4) mV as judged from the DPV.

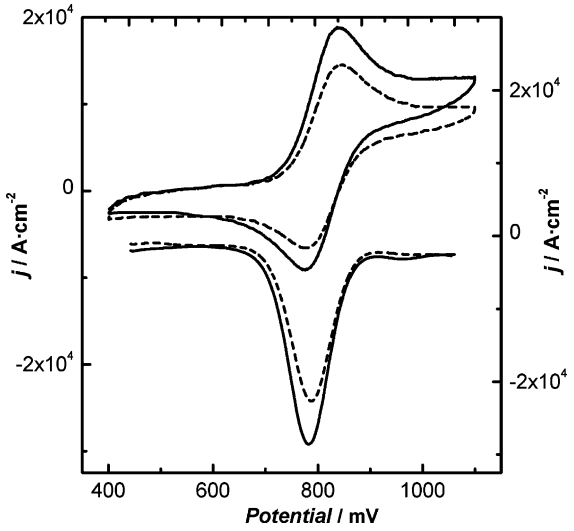

Fig. 4. CV and DPV. 5 mM solutions of compounds **1** (solid line) and **2** (dashed line) in MeOH 0.1 M TBAP.

Although peptide substituents allow for the electronic communication between a Fc redox group and a podand peptide, in compounds **1** and **2**, the removal of the ester protecting group has no measurable effect on the $E_{1/2}$, in line with the ^{13}C and UV–Vis results.

We and others showed that the halfwave potential of the ferrocene group in ferrocene-conjugates having ionizable groups is pH dependent [26,27]. Fabbrizzi and co-workers [27] showed that protonation will influence the redox potential of ferrocene carboxylic acid. The redox potentials of the Fc–COOH and its conjugated base Fc–COO^- are significantly different (Fc–COOH $E^o = 5.28$ mV; Fc–COO^- $E^o = 337$ mV versus sat't calomel). Measurements on a series of compounds of the type Fc–$(CH_2)_n$–COOH ($n = 0$–2) showed that the peak separation between the oxidation and reduction peak is reduced as the aliphatic chain length increases. This is directly related to the differences in pK_a of the acid and its conjugated base. As the aliphatic chain length increases the difference in pK_a between acid and conjugates base decreases as the electronic communication is reduced.

We carried out titration experiments of the free acid **2** in phosphate buffer between pH 2 and 8. Fig. 5(a) shows two CV recorded at pH 2 and at pH 8. The redox process remained fully reversible over the entire pH region ($\Delta E = 50$–69 mV; $i_a/i_c \sim 1$), indicating that the redox system was under thermodynamic control with respect to proton transfer [28]. The $E_{1/2}$ decreases from 690 mV at pH 2–647 mV at pH 8.0. A plot of $E_{1/2}$ as a function of pH is shown in Fig. 1 together with the nonlinear least square fit to Eq. (1). Thus, at $pH < 3$ compound **2** remains largely protonated, whereas at higher pH, compound **2** is completely deprotonated. The CV titration does not allow to distinguish between a stepwise deprotonation involving the mono-deproto-

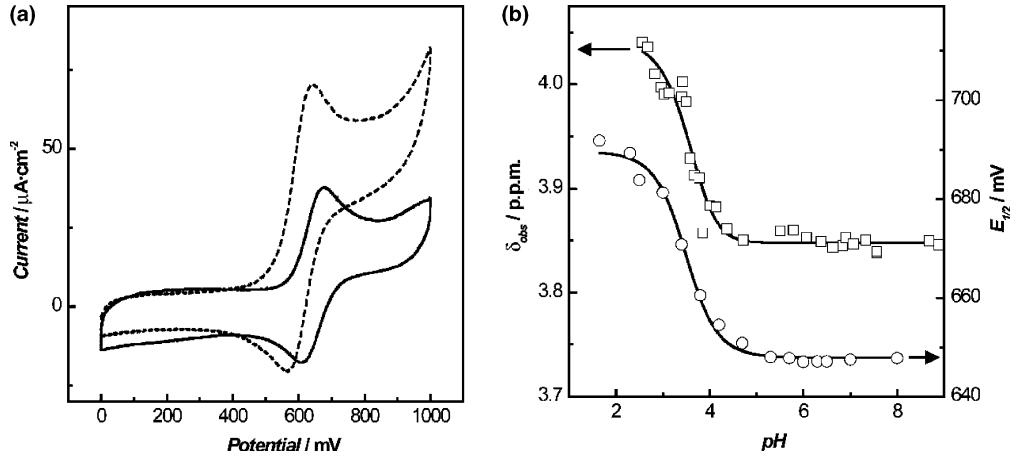

Fig. 5. pH dependence of the halfwave potential $E_{1/2}$ (a) CV of **1** at pH 2 (solid line) and pH 8 (dashed line). (b) ^{1}H NMR (?) and electrochemical (?) dependence on pH. $T = 25$ °C, glassy carbon electrode, Ag/AgCl reference electrode and Pt counter electrode 0.5 mM in 2.0 M phosphate buffers pH 2–8) and the influence of pH on the chemical shift δ of the CH_2 of the Gly substituent (?) for 1,1′-Fc(Gly-OH)$_2$ (**2**) ($T = 25$ °C).

nated species Fc(Gly-O$^-$)(Gly-OH) and fully deprotonated Fc(Gly-O$^-$)$_2$. The curve fit to Eq. (1) allows us to obtain the pK_as for protonation/deprotonation equilibrium of the oxidized and reduced species. A pK_a for Fc(Gly-OH)$_2$ of 3.8 ± 0.2 and a pK_a of 3.3 ± 0.2 for [Fc(Gly-OH)$_2$]$^+$ was obtained. Oxidation of the Fc group results in a higher acidity of the acid group, which results in a larger value for the pK_a of the oxidized species. The equilibrium is shown in Scheme 2.

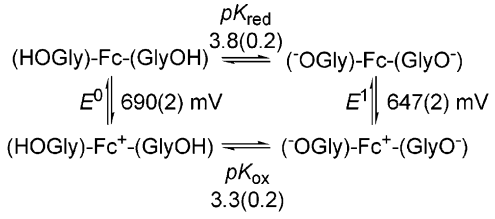

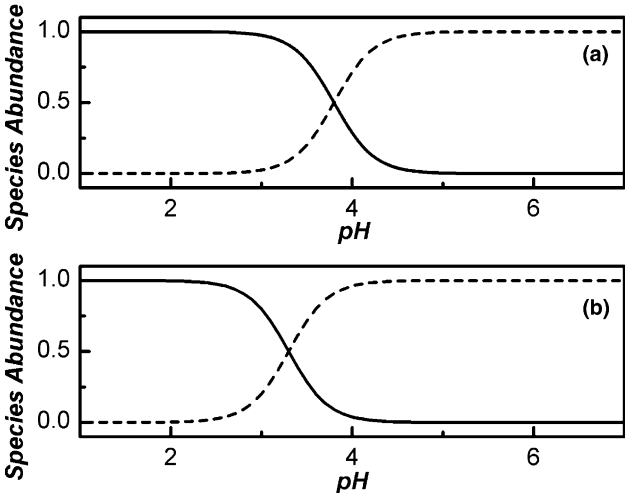

Scheme 2. Redox protonation–deprotonation pathway for Fc(Gly-OH)$_2$ (**2**) and it associated speciation representation at reductive potentials, (a), and oxidative potentials, (b).

$$E = E^{o}_{1/2} + RT/nF \ln[K_{red} + H^+/K_{ox} + H^+]. \quad (1)$$

These pK_a values compare favorably to pK_as obtained from NMR titration experiments, in which the chemical shift of the methylene group of Gly was flowed over the pH range of 2–8 (see Fig. 2). Importantly, both pH titrations give identical pK_a values for the free acid **2** of 3.8 ± 0.2 (electrochemical; 3.8 ± 0.15 for NMR). Similar to the electrochemical studies, the NMR titration experiments do not allow to distinguish between two separate deprotonation events. We interpret this to mean that the pK_a of both protons is identical or close to identical. The absolute value of the pK_a is in good agreement with values reported before for the pK_as of pyruvic acid (3.2–3.9) and other N-substituted glycines (3.75–4.07) [29–31].

4. Summary and conclusions

In this paper, we reported the solid state structures of Fc(Gly-OEt)$_2$ **1** and Fc(Gly-OH)$_2$ **2** – two disubstituted peptide ferrocene conjugates – which display very distinctive H-bonding patterns. It is possible to influence and to control the H-bonding in 1,1′-bis-amino acid-substituted ferrocenes. Deprotection of the acid group by base hydrolysis results in a conformational change that is accompanied by a dramatic change in the H-bonding pattern. It must be stressed at this point that in contrast to other reported ferrocene–peptide conjugates, the ester **1** adopts a 1,3′-conformation allowing extensive intermolecular H-bonding to adjacent molecules forming 1-D chains. Related esters exhibit exclusively a 1,2′-conformation, which in most cases displays cross-strand H-bonding. In contrast, the H-bonding in the free acid **2** is more in line with Hirao's reports of

disubstituted ferrocene peptides having a 1,2′-conformation allowing intramolecular H-bonding involving the two amides on opposite Cp rings. Of course, significant changes in the H-bonding might be expected when going from esters to acids, predicting these changes a priori is currently not possible.

What are the principles governing this change in the H-bonding pattern? This observation cannot be explained by steric effects. If steric bulk was responsible bulkier substituents, such as Val, may be expected to adopt the potentially more favorable 1,3′-conformation. Why does it not engage in interstrand interactions? Val is known for its high β-sheet preference [32]. Despite the bulk, Fc[Val-OMe]$_2$ it adopts 1,2′-conformation, even lacking the stabilizing H-bonding interactions. Other Fc–Gly-peptides also adopt the 1,2′-H-bonded conformation. Thus there is nothing inherent in preventing Gly from adopting this conformation. Metzler-Nolte's Phe derivative displays a single cross-strand H-bond and not two. Thus, sterics are not responsible for this behavior, nor is the system driven by intramolecular H-bonding. Although intramolecular interactions are important, they are not the guiding principles that govern the association of the molecules in the solid state of even in solution. Given the current knowledge, we would expect that upon deprotection of Fc[Phe-OMe]$_2$ and Fc[Val-OMe]$_2$ give raise to intramolecular H-bonded systems having a compact 1,2′-conformation, which interacts with adjacent molecules. We are currently engaged in experiments addressing this issue in order to fully understand the guiding principles that drive this process.

5. Supporting information available

CIF files for compounds **1** and **2**. VT ^{1}H NMR of compounds **1** and **2**.

Acknowledgements

This work was supported by the National Science and Engineering Research Council of Canada (NSERC). H.B.K. is the Canada Research Chair in Biomaterials. Financial support in the form of a Commonwealth Scholarship to F.A. is gratefully acknowledged. We thank Bob McDonald, X-ray Crystallography Laboratory, Department of Chemistry, University of Alberta, for collecting the data set for compound **1** and **2**.

References

[1] H. Mihara, Y. Haruta, S. Sakamoto, H. Aoyagi, Chem. Lett. 1 (1996) 1–2.
[2] C.A. Mirkin, R.L. Letsinger, R.C. Mucic, J.J. Storhoff, Nature 382 (1996) 607.
[3] A.P. Alivisatos, K.P. Johnsson, X. Peng, T.E. Wilson, C.J. Loweth, M.P. Bruchez, P.G. Schultz, Nature 382 (1996) 609.
[4] (a) M. Engles, D. Bashford, M.R. Ghadiri, J. Am. Chem. Soc. 117 (1995) 9151;
(b) J.R. Granja, L. Castedo, J. Am. Chem. Soc. 125 (2003) 2844–2845;
(c) M.R. Ghadiri, M.P. Isler, J. Sanchez-Quesada, J. Am. Chem. Soc. 124 (2002) 10004–10005;
(d) W.S. Horne, C.D. Stout, M.R. Ghadiri, J. Am. Chem. Soc. 125 (2003) 9372–9376.
[5] for example: C.B. Aakeroy, K.R. Seddon, Chem. Soc. Rev. 22 (1993) 397–407.
[6] (a) T. Moriuchi, A. Nomoto, K. Yoshida, T. Hirao, J. Organomet. Chem. 589 (1999) 50–58;
(b) K. Plumb, H.-B. Kraatz, Bioconjugate Chem. 14 (2003) 601–606.
[7] T. Moriuchi, T. Tamura, T. Hirao, J. Am. Chem. Soc. 124 (2002) 9356–9357.
[8] P. Saweczko, G.D. Enright, H.-B. Kraatz, Inorg. Chem. 40 (2001) 4409–4419.
[9] (a) A. Nomoto, T. Moriuchi, S. Yamazaki, A. Ogawa, T. Hirao, Chem. Commun. (1998) 1963–1964;
(b) T. Moriuchi, K. Yoshida, T. Hirao, Organometallics 20 (2001) 3101–3105;
(c) T. Moriuchi, A. Nomoto, K. Yoshida, T. Hirao, Organometallics 20 (2001) 1008–1013;
(d) T. Moriuchi, A. Nomoto, K. Yoshida, A. Ogawa, T. Hirao, J. Am. Chem. Soc. 123 (2001) 68–75;
(e) T. Moriuchi, K. Yoshida, T. Hirao, J. Organomet. Chem. 668 (2003) 31–34.
[10] D.R. van Staveren, T. Weyhermüller, N. Metzler-Nolte, Dalton Trans. (2003) 210–220.
[11] R.S. Herrick, R.M. Jarret, T.P. Curran, D.R. Dragoli, M.B. Flaherty, S.E. Lindyberg, R.A. Slate, L.C. Thornton, Tetrahedron Lett. 37 (1996) 5289–5292.
[12] M. Oberhoff, L. Duda, J. Karl, R. Mohr, G. Erker, R. Fröhlich, M. Grehl, Organometallics 15 (1996) 4005–4011.
[13] G. Schachschneider, M.J. Wenzel, J. Labelled Comp. 12 (1985) 235–244.
[14] D. Braga, F. Grepioni, Chem. Soc. Rev. 29 (2000) 229.
[15] (a) G.J. Palenik, Inorg. Chem. 8 (1969) 2744–2749;
(b) F. Takusagawa, T.F. Koetzle, Acta Crystallogr. B B35 (1979) 2888–2896.
[16] (a) D. Braga, L. Maini, F. Paganelli, E. Tagliavini, S. Casolari, F. Grepioni, J. Organomet. Chem. 637–639 (2001) 609–615;
(b) C.M. Zakaria, G. Ferguson, A.J. Lough, C. Glidewell, Acta Crystallogr. B 58 (2002) 786–802.
[17] A.S. Georgopoulou, D.M.P. Mingos, A.J.P. White, D.J. Williams, B.R. Horrocks, A. Houlton, J. Chem. Soc., Dalton Trans. (2000) 2969–2974.
[18] (a) O.R. Evans, W. Lin, Acc. Chem. Res. 35 (2002) 511–522;
(b) B. Moulton, M.J. Zaworotko, Chem. Rev. 101 (2001) 1629–1658;
(c) G.R. Desiraju, Crystal Engineering: the Design of Organic Solids, Elsevier, New York, 1989;
(d) D. Braga, F. Grepioni, Acc. Chem. Res. 33 (2000) 601–608;
(e) G. Desiraju, Chem. Res. 35 (2002) 565–573.
[19] (a) J.M. Lehn, Science 295 (2002) 2400–2403;
(b) D.N. Reinhoudt, M. Crego-Calama, Science 295 (2002) 2403–2407;
(c) O. Ikkala, G. ten Brinke, Science 295 (2002) 2407–2409;
(d) M.D. Hollingsworth, Science 295 (2002) 2410–2413;
(e) T. Kato, Science 295 (2002) 2414–2418;
(f) G.M. Whitesides, B. Grzybowski, Science 295 (2002) 2418–2421.

[20] (a) G.M. Sheldrick, Acta Crystallogr. A 46 (1990) 467–473;
(b) G.M. Sheldrick, SHELXS-97, University of Göttingen, Germany, 1990;
(c) G.M. Sheldrick, SHELXL-93, University of Göttingen, Germany, 1993.
[21] H.-B. Kraatz, J. Lusztyk, G.D. Enright, Inorg. Chem. 36 (1997) 2400–2405.
[22] I. Bediako-Amoa, R. Silerova, H.-B. Kraatz, Chem. Commun. (2002) 2430–2431.
[23] T. Moriuchi, K. Yoshida, T. Hirao, J. Organomet. Chem. 637–639 (2001) 73–79.
[24] L. Lin, A. Berces, H.-B. Kraatz, J. Organomet. Chem. 556 (1998) 11–20.
[25] G.R. Desiraju, The Weak Hydrogen Bond, Oxford University Press, Oxford, 1999.
[26] M. Chahma, J.S. Lee, H.-B. Kraatz, J. Organomet. Chem. 648 (2002) 81–86.
[27] G. De Santis, L. Fabbrizzi, M. Lichelli, P. Pallvicini, Inorg. Chim. Acta 225 (1994) 239–244.
[28] A.N. Moore, D.D.M. Wayner, Can. J. Chem. 77 (1999) 681–686.
[29] A.J. Kresge, J. Pure Appl. Chem. 63 (1991) 213–221.
[30] A. Bryson, N.R. Davies, E.P. Serjeant, J. Am. Chem. Soc. 85 (1963) 1933–1938.
[31] K. Curley, R.F. Pratt, J. Org. Chem. 62 (1997) 4470–4483.
[32] C.K. Smith, L. Regan, Acc. Chem. Res. 30 (1997) 153–161.